Physics – Uspekhi **40** (10) 1019 – 1034 (1997)

REVIEWS OF TOPICAL PROBLEMS PACS numbers: **05.90.+m**, 64.60.My, 64.70.Ja

Studies of spinodal decomposition in stratified solutions using laser methods

N F Bunkin, A V Lobeev, G A Lyakhov

Contents

Abstract. Self-excited spinodal decomposition oscillations are obtained in a binary, liquid, stratified mixture deep in the labile region. An opto-thermodynamic method is presented for locating the binodal and the spinodal in the temperature-concentration plane for stratified solutions with a lower critical point. It is shown that light-induced barodiffusion serves as an effective mechanism for quenching a stratified solution into the metastable region.

1. Introduction

Studies of liquid solutions (here and later we shall consider only binary solutions) attracted interest because of the possibility of stratification phase transition upon changing the concentration u or the temperature T, many specific features of this phenomenon being unclear. One of the problems is associated with the existence of solutions that reveal anomalous behaviour with changing temperature T: the separation into two phases occurs not upon cooling (when the efficiency of mixing decreases) but upon heating (see, for example, Refs [1, 2]). The (u, T) phase diagram of such solutions is characterized by a lower critical point (LCP). Such anomalous behaviour can be qualitatively explained as follows. Upon mixing of associated (forming intermolecular bonds) liquids A and B, which are characterized by LCP stratification, the entropy effects caused by the formation of 'direct' (A – A and B – B) and 'cross' (A – B) bonds between the molecules compete with Brownian mixing (the model of stochastic bonds for a liquid phase was proposed in Ref. [3]). Because in general, the efficiency of Brownian mixing and the entropy effects depend differently on the temperature, their simultaneous action can result in a nonmonotonic dependence on T of the solubility of components. However, it is clear that in the low-temperature region the solution should segregate into two phases (the Brownian mixing efficiency is infinitesimal.) It is also obvious that at sufficiently high temperatures, the intense Brownian motion breaks the intermolecular bonds and stratification does not occur. As a result, the general (u, T)-plane phase diagram should appear as in Fig. 1 [4] (the number of closed stratified regions is determined by the number of types of intermolecular bonds.) The low-temperature part (adjacent to the u-axis) of the stratification phase diagram may be found in the crystallization region; the high-temperature part, in turn, may correspond to the gaseous phase. For this reason, the phase diagrams shown in Fig. 2 are more often realized; they represent fragments of the complete phase diagram, which are bounded above by the boiling temperature and below, by the crystallization temperature of the mixture.

At present, a consistent microscopic theory of associated solutions is absent, although numerous experimental results on the kinetics of such solutions are available. In addition, along with scientific studies, the associated water solutions attract interest because of their numerous technological applications.

A phase diagram of the solution contains a binodal (this is the boundary between the stable and metastable states) and a spinodal which bounds the region of absolutely unstable (labile) homogeneous states. On the binodal, the chemical potentials of two equilibrium phases are equal: $\mu_1 = \mu_2$. On the spinodal, the condition

$$\frac{\partial \mu_1}{\partial u_1} = \frac{\partial \mu_2}{\partial u_2} = 0$$

N F Bunkin, A V Lobeev, G A Lyakhov Institute of General Physics, Russian Academy of Sciences,
ul. Vavilova 38, 117942 Moscow, Russia
Tel. (7-095) 952 05 40. Fax (7-095) 135-82 34
E-mail: nbunkin@kapella.gpi.ru

Received 24 February 1997, revised 15 May 1997
Uspekhi Fizicheskikh Nauk **167** (10) 1069 – 1085 (1997)
Translated by M N Sapozhnikov; edited by A Radzig

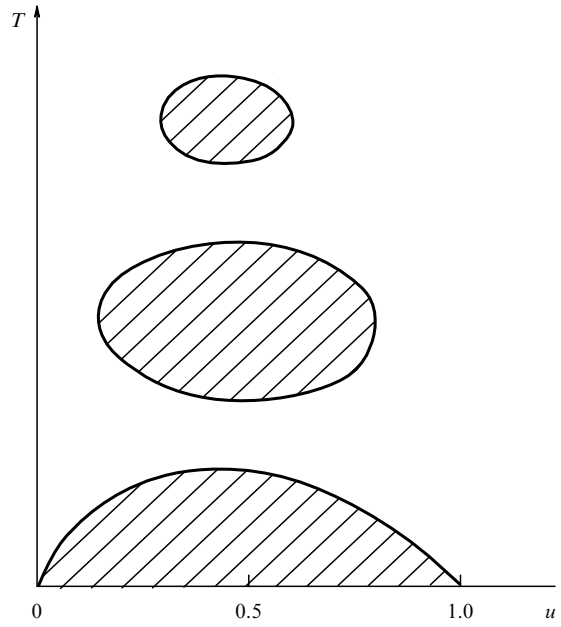

Figure 1. General phase diagram of a phase separable solution in concentration – temperature coordinates.

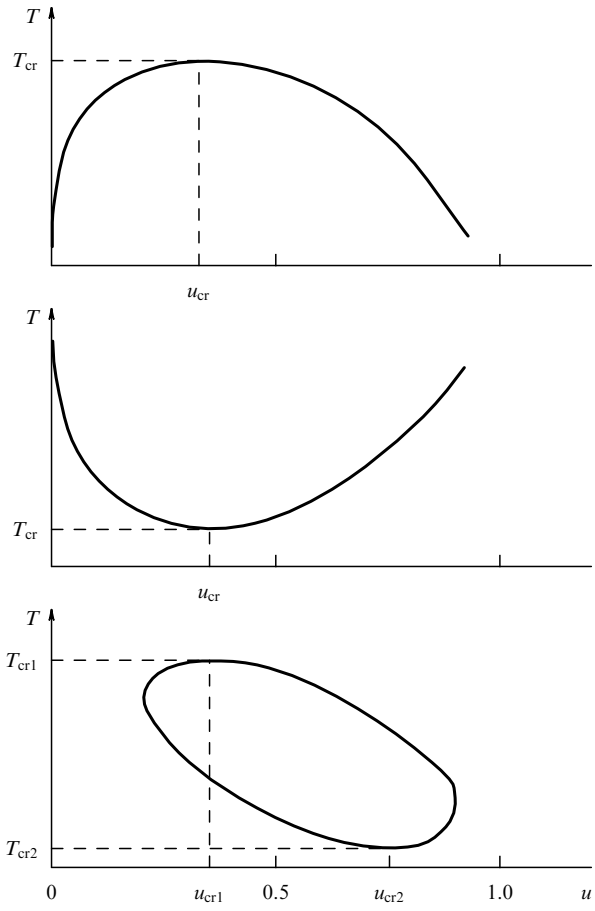

Figure 2. Phase separation curves for solutions with (a) an upper critical point (UCP), (b) a lower critical point (LCP), and (c) a closed curve (with a UCP and an LCP).

is satisfied, where $u_{1,2}$ are the molar fractions of the components of the solution, and $u_1 + u_2 = 1$. The coefficient of mutual diffusion D of these components is proportional to $\partial\mu_{1,2}/\partial u_{1,2}$. For this reason, diffusion transfer sharply slows down on approaching the spinodal. In region I, outside the binodal (Fig. 3), the state with homogeneous spatial concentration distribution is stable; in the metastable region II, diffusion causes motion to one of the homogeneous states standed out by spontaneous violation of symmetry — to a nucleus of the conjugate phase. At the critical point, the spinodal touches the binodal. The labile region III, which comprises, together with the metastable and stable regions, the complete set of possible phase states of the substance, is the least known both experimentally and theoretically. It is known that if the system can be quenched into the labile state, its subsequent relaxation to the stable heterophase state may occur via a particular nonequilibrium phase transition, which is called a spinodal decomposition (SD) [5]. The SD process is characterized by the 'enhancement' of random inhomogeneities, resulting in the appearance of a granular relaxation structure without phase boundaries in the early stages. In the later stages, the usual heterogeneity appears: one of the phases is dispersed inside the other in the presence of a stable interfacial boundary (which, of course, has a complicated topology.)

The SD theory [6–11] modified in Refs [12–14] (in particular, for polymer solutions) assumes that the concentration u of any component (the subscripts '1' and '2' for u will be omitted below) differs only slightly from the average concentration u_0 at each point of the solution. A change in the concentration is described in the first approximation by the linearized diffusion equation

$$\frac{\partial u}{\partial t} = L\nabla^2(\chi^{-1} - 2K\nabla^2 u)\,, \tag{1.1}$$

whose solution can be represented by the Fourier series [5]

$$u(\mathbf{r}, t) - u_0 = \sum_{\mathbf{k}} A(\mathbf{k}, t)\exp(\mathrm{i}\mathbf{k}\cdot\mathbf{r})\,, \tag{1.2}$$

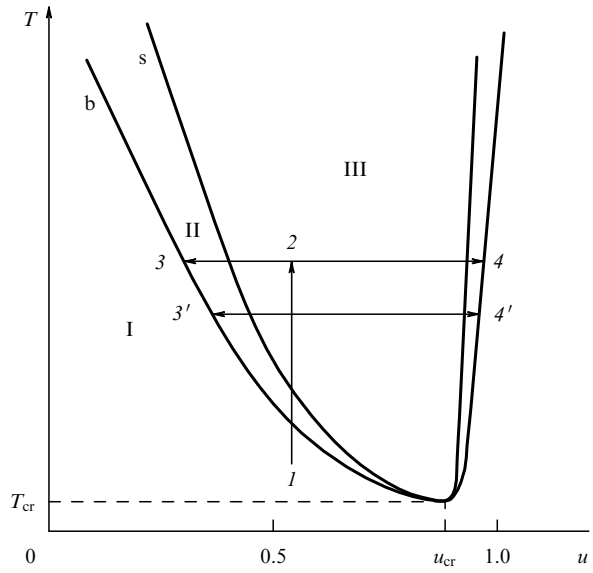

Figure 3. Phase diagram of a phase separable solution with the LCP; the indicated regions correspond to stable, metastable, and labile states.

where

$$A(\mathbf{k},t) = A(\mathbf{k},0)\exp\left[R(k)t\right], \qquad (1.3)$$
$$R(k) = -Lk^2(\chi^{-1} + 2Kk^2).$$

Here, $L = L_{11} > 0$ is the kinetic Onsager coefficient characterizing the mobility of molecules, $\Delta\mu = \mu_1 - \mu_2$ is the difference between the chemical potentials of components of the solution, $K = D/2L$, and $k = |\mathbf{k}|$ is a basis set of wave numbers corresponding to elementary concentration modes, and $\chi = \partial u/\partial(\Delta\mu)$. In the labile region $\chi < 0$, so that the increment $R(k)$ is positive for $k < k_c = (-2K\chi)^{-1/2}$ and reaches its maximum value at $k = k_m = k_c/\sqrt{2}$.

In optical experiments, the scattered light intensity $I(\mathbf{q},t)$ is usually observed, where $\mathbf{q}$ is the scattering wave vector, $|\mathbf{q}| = (4\pi/\lambda)\sin(\theta/2)$, λ is the radiation wavelength, and θ is the angle between the incident and scattered beams. By assuming that $\mathbf{q} = \mathbf{k}$, we obtain $I(\mathbf{q},t) \propto \left|A(\mathbf{q},t)\right|^2$ in the Born approximation [15]. Therefore, the measurement of $I(\mathbf{q},t)$ yields direct information on the spatial spectrum of the concentration fluctuations in the system. In the linearized theory, the scattered light intensity $I(\mathbf{q},t)$ is described, according to (1.3), by the expression

$$I(\mathbf{q},t) = I(\mathbf{q},0)\exp\left[2R(q)t\right], \qquad (1.4)$$

i.e. the theory predicts an exponential growth of I for $q < q_c$ and an exponential decay of I for $q > q_c$. The scattered light intensity has a maximum in the direction of q_m, which is determined by a maximum of the increment. It is this behaviour of the structures formed in the early stages of the SD that is observed, as a rule, in experiments, and the simple expression (1.4) can be used as the basis for experimental verification of the linearized SD theory.

Spinodal decomposition in binary liquid solutions undergoing stratification was first observed in Ref. [16]. The phase separation in a binary mixture of methanol and cyclohexane near the critical point was studied from scattering of radiation from a He – Ne laser in a cell several centimetres in length. The angular distribution of the scattered light intensity was registered with photomultipliers and also on photographic film. The labile state was produced by changing the solution temperature. The depth of quench into the labile region was $\Delta T = |T - T_{cr}| = 2 \times 10^{-3}$ K, where T_{cr} is the critical temperature. After quenching the system into the labile state, along with the central dark spot produced by the traversed laser beam, a ring caused by scattering from the short-range order structure appeared on the photographic film placed in the far field perpendicular to the incident laser beam. The development of a ring suggests the appearance of an ordered structure with characteristic size $\lambda_m = 2\pi/q_m$. It was found that roughly 1 min after the quench into the labile area, the scattered light intensity was $I(t) \propto \exp\left[2R(q_m)t\right]$, while the radius of the ring was constant. After a lapse of several minutes the radius of the ring decreased and then the ring collapsed, corresponding to the increase in the system scale.

Thus, the process observed in Ref. [16] is related to the early stage of SD. Notice here that an interesting method for quenching a binary liquid into the labile state was proposed in Ref. [17]. It is based on the dependence of the temperature T_{cr} on pressure. A critical mixture of isobutyl acid and water was quenched into the labile region by quickly changing the pressure at constant temperature. In contrast to Ref. [16], in Ref. [17] the scattered light intensity $I(t)$ did not grow exponentially even in the early stages of the spinodal decomposition. The experimental data [17] can be considered reliable because a quick quench into the labile region was produced, which avoided any difficulties related to the finite time of establishing thermal equilibrium. Note that the time of the diffraction ring persistence decreases with increasing depth of the quench. The short observation time substantially limits the possibilities of studying SD.

The SD theory based on a linearized diffusion equation can be applied, as was mentioned above, only to the early stages of decomposition when concentration fluctuations are small. In the later stage, the assumption of the smallness of $u - u_0$ becomes invalid because of its continuous growth. In this stage, the time dynamics of the scattered light intensity is described by a power function $I(t) \propto t^{\beta}$ [18–23], the exponent β being dependent on both the time and depth of the quench into the labile region (in Ref. [18], a regime with the exponent β invariable in time was specially distinguished.) An experimental method analogous to that described in Ref. [16] was applied for studying SD in a solution of 2-6-lutidine and water with a LCP [24, 25]. It was shown that at distinct stages of SD, the approximation $I(t) \propto t^{1/3}$ is valid for all depths of the quench studied. In Ref. [26], the kinetics of SD was also studied as a function of the depth of quench and the dependences $q_m(t)$ and $I\left(q_m(t)\right)$ at $\Delta T < 2 \times 10^{-3}$ K were found to be well described by a power law in t predicted by the theory of Kawasaki [21]. For $\Delta T \geqslant 2 \times 10^{-3}$ K, the agreement between theory and experiment disappears, which can be explained by the finite rate of temperature variation in the experiment.

In the developed stage of SD, a further growth of scattering structures (droplets of one of the phases dispersed in the other phase) occurs, and the dependence $I(t)$ is described by the transcendental equation of Furakawa [22]. An interesting feature of SD dynamics was found in Ref. [18]. In the initial stage, the scale of the droplets is characterized by the only time-dependent quantity — the size R of a droplet of the conjugate phase. However, when the concentration in the central regions of droplets is at equilibrium and is still far from equilibrium at their boundaries, another time-dependent spatial scale appears — the thickness d of the interface layer. Lastly, the concentration drop in the interface layer at the final stage of SD is so large that d becomes independent of t, and again only one spatial scale $R(t)$ is dependent on t. (We shall show below in Section 2.2 that the 'time return' during SD is a fundamental property of this phenomenon.) It follows from the above brief (and far from complete) review of papers on SD dynamics that this problem is not yet fully understood.

A phase separable solution can be also quenched into the labile state by the thermal action of radiation. For example, this was done in an LCP water solution of triethylamine and butyl Cellosolve heated in the course of volume energy release by absorption of high-power radiation [27, 28]. The separate stages of SD were studied using a single-pulse Nd^{3+}:YAG laser. Different SD regimes with a finite quenching rate were realized using pulse trains from a free-running Nd^{3+}:YAG laser and from the broadband radiation of a pulsed xenon lamp. This method for quenching a solution into the labile state provided a significant increase in the quenching depth and rate, resulting in a substantial acceleration of the relaxation diffusive processes. It was shown that under the action of powerful radiation, photo-induced concentration structures appear in the absorbing solutions undergoing

stratification. This provides a mechanism of photo-induced diffusion redistribution of the components and the enhancement of this effect, inherent in liquid mixtures upon quenching. Under certain conditions the photo-induced concentration structures play the role of a nucleator of SD. In Ref. [29], the contributions of the spontaneous self-diffusion and photo-induced diffusion mechanisms related to thermal diffusion and barodiffusion, thermal conductivity and photo-induced variation in $\Delta\mu$ were determined. The early and late stages of SD were studied in Ref. [29] not only from the dynamics of a 'spinodal ring' in the scattering pattern but also from a change in the extinction coefficient of the probing radiation. In the early stage, the extinction coefficient grows linearly with time ($\propto \Gamma t$), where $1/\Gamma$ is the time of appearance of the modulated spatial structure; Γ depends on the heat supply rate $q \sim \mathrm{d}Q/\mathrm{d}t$ as $\Gamma \propto q^{\psi}$, where $\psi = 0.65$.

An interesting method for quenching a phase separable solution into the labile region was suggested in Ref. [30]. A binary mixture of methanol and heptane with an upper critical point was transferred, upon cooling, from the subcritical to the supercritical region. The solution stratification caused by convective separation of heavy and light components should start on entering the binodal. The stratification was suppressed by vigorously stirring the liquid, which provided a fairly long persistence time for the supercritical state.

In conclusion, we note a number of papers [31 – 34] devoted to studies of SD in polymer solutions. The rate of spreading of the ordered SD structure due to the convection countercurrent of light and heavy phases in such solutions is small because of their high viscosity. For the same purpose, liquid mixtures were used in which the densities of the fractions formed upon phase separation were close [18, 35].

2. Studying dynamics of spinodal decomposition for a deep quench into the labile region

The SD of a liquid solution for a deep quench into the labile region and the time dynamics of this process were studied in Refs [36, 37]. The kinetics of SD in a phase separable water solution of 2,4,6-trimethylpyridine (TMP) (the phase diagram of the TMP solution in water taken from handbook [38] is presented in Fig. 4) was studied using a low-power ($I \approx 2 \times 10^{-3}$ W cm^{-2}) He – Ne-laser radiation. The development of the spatial SD structure was monitored from the angular spectra of the laser radiation scattered in a cell of the liquid under study. Physical properties of the TMP solutions are substantially determined by the kinetics of the hydrogen bonds between nitrogen atoms of the pyridine rings in TMP molecules and the hydrogen atoms of the water molecules. In particular, these bonds exhibit solution stratification upon heating (the lower critical point of the solution is $T_{\mathrm{cr}} = 5.7\,^{\circ}$C.) Aqueous solutions of methylpyridines are convenient for studies because the refractive indices of their components substantially differ ($|\Delta n| \approx 0.2$), while their densities are close, resulting in a diminished convection effect.

2.1 Experimental method of studying spinodal decomposition for a deep quench into the labile region

As was mentioned above, SD is the process of a system relaxation to the equilibrium, and it is observed under the non-stationary conditions characterized by a certain set of time scales (see, for example, Ref. [5]). To evaluate the depth of quench $\Delta T = |T - T_{\mathrm{cr}}|$ into the labile region that can be

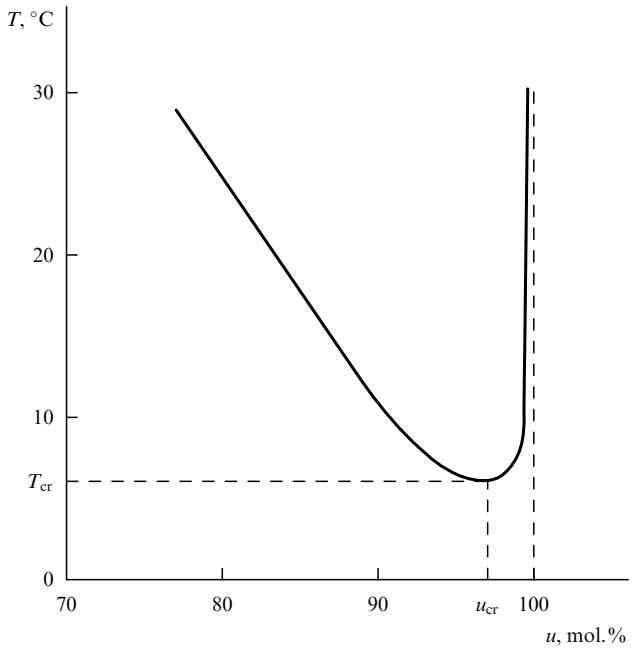

Figure 4. Phase diagram of a water solution of 2,4,6-trimethylpyridine.

achieved during the observation time $\mathcal{T}$, one should know the average time $\langle\tau\rangle$ for the appearance of a nucleus in the volume element ΔV and the phase separation time τ_{s} in this volume element in the presence of the nucleus. Because the times $\langle\tau\rangle$ and τ_{s} sharply decrease with increasing ΔT, the maximum value of ΔT that can be achieved in the experiment is determined by the condition

$$\mathcal{T} \lesssim \langle\tau\rangle + \tau_{\mathrm{s}}\,.$$

Therefore, in order to observe SD in passing from the state *1* to the point *2* (see Fig. 3), the temperature should be changed rather quickly lest the diffusion has time to increase the nuclei of conjugate phases (the *3*, *4*, and all other intermediate states of the *3′*, *4′* types) to the size critical of solution stratification caused by convection. This condition becomes more stringent with increasing ΔT: in a cell 1 cm in length, the solution undergoes stratification at $\Delta T \sim 10^{-3}$ K in 15 min and at $\Delta T \sim 1$ K, in one second. For this reason, the possibilities of the known experiments on SD observation (see Introduction) are limited (in the case of nonviscous solutions) by the condition imposed on the times $\langle\tau\rangle$ and τ_{s}, which is difficult to satisfy. Hence, the conclusion about the monotonic in time dynamics of decomposition is only valid within a quite short time interval. On the other hand, the monotonic behaviour of the SD process, which has a diffusion nature, directly follows from the assumption that the difference $u - u_0$ is small.

An alternative approach [36, 37] consists in using a thin-layer vertical cell (the distance between cell windows $d = 25$ μm) for the solution under study. Convective flows in a cell of such a size, which appear upon heating the liquid, are negligibly small [37]. Indeed, by neglecting the temperature gradient ∇T along the gap between the cell windows, we can express ∇T along a radius $R = 1$ cm of the cell windows in the form $(\nabla T)_{\mathrm{r}} \cong \delta T/\sqrt{4\chi t}$, where δT is the difference between the temperature of the window ends (which are adjacent to a water jacket of the cell and whose temperature corresponds to

the maximum one, see Section 2.2) and the temperature at the centre of the window at the beginning of heating, χ is the thermal conductivity either of the liquid or the cell window material (we should insert the maximum of these two values), and t is the heating time. Notice that the value δT measured in this way in fact corresponds to the depth of quench ΔT into the labile region (this will be clear from a description of the experiment.) The convective counterflow is absent if the development time τ_{conv} of the convective instability exceeds the time $R^2/4\chi$ of liquid heating, i.e. the time of the gradient $(\nabla T)_r$ existence. The time τ_{conv} can be evaluated in the following way. The velocity u of a liquid particle of density ρ' and volume V, which floats up under the action of Archimedes' force, being inside a liquid of the same viscosity but of greater density $\rho > \rho'$, is equal to

$$u \approx \frac{gV^{2/3}}{10v}\left(1 - \frac{\rho'}{\rho}\right),$$

where $v = \eta/\rho$ is the kinematic viscosity, and g is the acceleration due to gravity (see, for example, Ref. [39]). The physical meaning of u is obvious: it is the mixing rate. Assuming that $1 - \rho'/\rho = \beta\delta T$, where β is the coefficient of thermal expansion (i.e. the density difference is caused by heating), and $V \approx d^2\sqrt{4\chi t}$, we define time τ_{conv} as the time during which a particle of volume V comes rise through the height R:

$$R = \int_0^{\tau_{conv}} u\,\mathrm{d}t\,.$$

Upon integrating, we obtain

$$\tau_{conv} \approx \left(\frac{5Rv}{g\beta\delta T}\right)^{3/4}\left(\frac{4}{\chi}\right)^{1/4}\frac{1}{d}\,.$$

The condition of the absence of convection $\tau_{conv} > R^2/4\chi$ can be expressed in the canonical form:

$$\mathrm{Ra} \equiv \frac{g\beta\delta T R^3}{v\chi} < \mathrm{Ra}_{cr} \equiv 8\left(\frac{4R}{d}\right)^{4/3},$$

where Ra is the Rayleigh number. In our case, $\beta\delta T \sim 10^{-3}$ (the variation range of T and experimental conditions are given below), $v \sim 10^{-2}$ cm^2 s^{-1}, and $\chi \approx 5 \times 10^{-3}$ cm^2 s^{-1} for fused quartz, of which the cell windows were made (for water, χ is three times smaller.) Thus, we obtain $\mathrm{Ra} = 2.3 \times 10^4 < \mathrm{Ra}_{cr} = 1.5 \times 10^5$, i.e. the convective counterflow should indeed be suppressed. Note that the value of Ra must actually be even smaller, because in our case the gap between cell windows is comparable with the thickness of the boundary layer, in which the liquid velocity decreases due to the presence of a hard wall, resulting in a greater effective value of v. The validity of the above consideration is confirmed by the fact that we did not observe homogeneous transparent layers formed upon separation of heavy and light fractions in the gravitational field. Therefore, in the case of suppressed convection the lifetime of the SD structures can be increased up to tens of minutes at $\Delta T \sim 1-10$ K. In this case, the suppression of convection itself, of course, does not affect the process of producing new phases. Another undeniable advantage of thin cells is that the multiple scattering effects can be safely neglected because the size of a droplet of the conjugate phase is comparable with the gap d. Finally, notice that SD was studied in thin cells in several papers (see, for example, Ref. [40]). However, we are not aware of papers where this process has been investigated for a deep quench into the labile region.

The heat balance equations in the SD state are solved, as a rule, in the average field approximation used for linearization of these equations. Upon a deep quench into the labile region, the kinetics can be nontrivial under the conditions of strong nonlinearity (taking into account the dependence of the relaxation times on the concentration), as in other self-organized systems (see, for example, Ref. [42]). For this reason, in this case the average field approximation cannot give correct results. To interpret the SD kinetics, which experimentally proved to be nonmonotonic [36, 37], a nonlinear theory was developed which qualitatively describes various kinetic regimes: relaxation to the equilibrium level, soliton propagation, and cnoidal waves.

2.2 Observation of spinodal decomposition in an associated water solution

Because mixing is in fact absent in a water solution of TMP (its concentration in our experiment was critical: $u_{cr} = 97$ mol.% of H_2O), there is no need for a quick temperature variation for deep quenching into the labile region, and the temperature was controlled with a conventional thermostat. The lower bound on the heating rate is determined by the rate of diffusion approach to the binodal. In other words, the solution is in the labile state while heating proceeds, i.e. SD develops under nonstationary in temperature conditions. Before the experiment, the temperature of the solution in a cell was maintained below T_{cr} with the help of a thermostat connected to the water jacket of the cell. Then, the solution was heated in the thermostat for several seconds to $T = 25-30\,^{\circ}$C, which corresponds to a deep quench into the labile region; the moment of switching thermostat on for warming up served as the initial time t of the experiment. The temperature front propagated radially from the cell window ends upon heating (Fig. 5). The time of heating the outer surface of windows was determined experimentally and comprised about 10 min. The liquid itself was heated faster (in approximately 5 min, see below) because it did not contact the air.

Figure 5 shows the schematic of the experimental setup. The radiation from a single-mode He–Ne laser *1* with a Gaussian beam profile, obtained with the help of a 'soft' diaphragm, and a plane front (the diameter of the spot formed by a telescope was ≈ 1.5 cm) passed through cell *2* containing the solution under study. A convergent lens *3* with a focal distance of 4 m and an aperture diameter of 22.5 cm was placed directly behind the cell. This lens formed a scattering pattern on the detector. It collected the light beams scattered not only by large-scale SD structures (i.e. the beams scattered at small angles) but also, owing to its large aperture, the beams scattered by small-scale SD structures. At the focus of this lens was placed a circular mask *4*, which completely blocked the direct unscattered light beam (the mask kept the uninformative direct light beam from entering the detector), and behind the mask a television camera *5* with an aperture diameter of 2 cm was positioned. In addition, individual parts of the cell were projected with the help of a microscope *6* to another television camera *7*. This allowed us simultaneously to observe the dynamics of development of the SD structures and study the angular spectrum of the laser beam scattering from them.

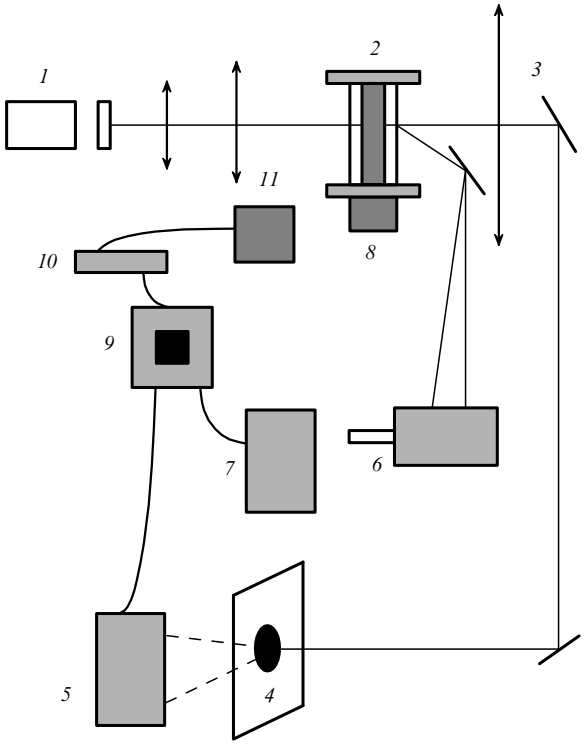

Figuure 5. Schematic of the experimental setup: (*1*) He – Ne laser; (*2*) cell of solution under study; (*3*) wide-aperture long-focus lens; (*4*) mask; (*5*, *7*) television cameras; (*6*) microscope; (*8*) thermostat; (*9*) television monitor; (*10*) analog-digital converter; (*11*) computer.

The photographs (Fig. 6), obtained with the help of the microscope, illustrate the SD dynamics. At the beginning (within time $t \sim 1$ min after switching on thermostat *8*), the SD wave front appears, which moves across the cell. Behind the wave front, small cellular structures of size 1 – 10 μm are observed (Fig. 6a), which gradually increase in size to ~ 100 μm over the entire observation field ($t = 2.5$ min, Fig. 6b) and, finally, associate to aggregates of size ~ 1 cm ($t = 5$ min, Fig. 6c).

The output signals of television camera *5* corresponding to the angular scattering spectrum were displayed on a television monitor *9*. The analog signal corresponding to the television picture on the monitor was digitized using an analog-digital converter *10* with the time interval of 1 or 5 s during the entire experiment (approximately for 20 min). The television picture digitized in this way is presented on the photograph in Fig. 7. The distinct circle at the left, which does not contain reflexes, corresponds to mask *4* blocking the direct laser beam; the light to the right from the mask image corresponds to scattering by the structures that appeared upon SD. The light reflexes located closer to the mask image relate to structures of larger sizes. The size of the scatterers can be determined exactly. For this purpose, we placed a diffraction grating with the known grating constant, instead of the cell with solution, and digitized its angular scattering spectrum. In this way we found the relation between the position of the reflex from a scatterer on the entrance pupil of the television camera and the scatterer size. The reflexes corresponded to sizes from 30 to 300 μm. The digitized signal was processed with a computer *11*, which read out the picture brightness along the separated television line (see Fig. 7). This brightness was strictly fixed during the experiment.

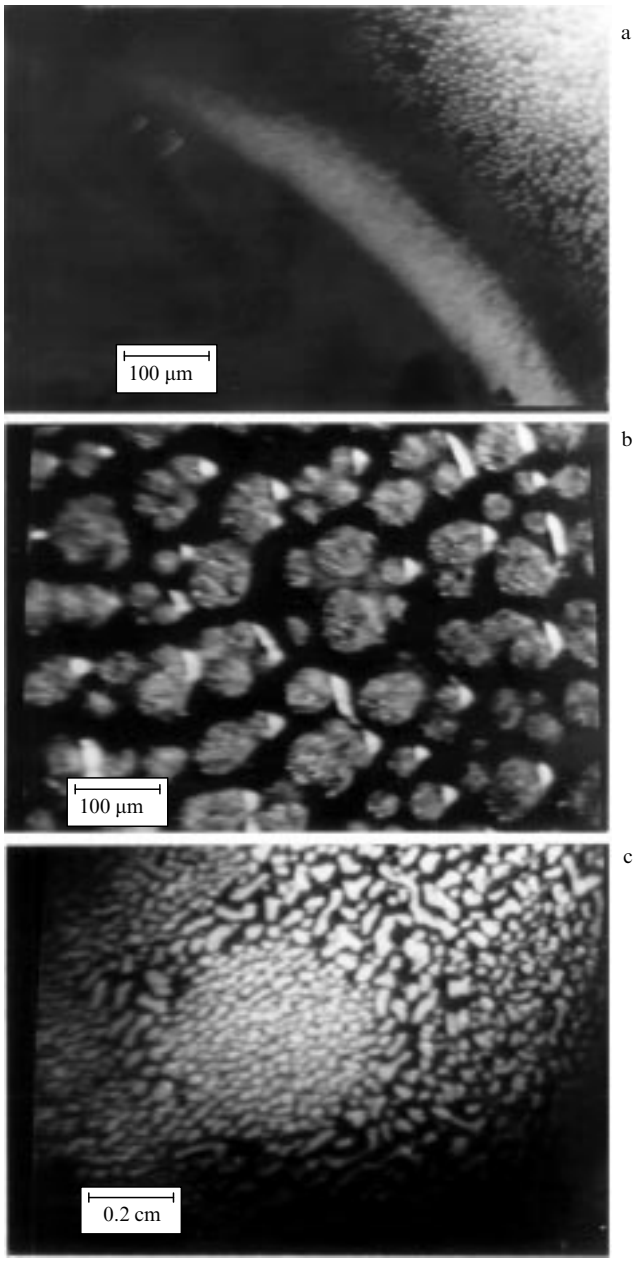

Figure 6. Microphotographs of spinodal decomposition at different moments after the onset of heating: (a) $t = 1$ min, scale 100 μm; (b) 2.5 min, scale 100 μm; (c) 5 min, scale 0.2 cm.

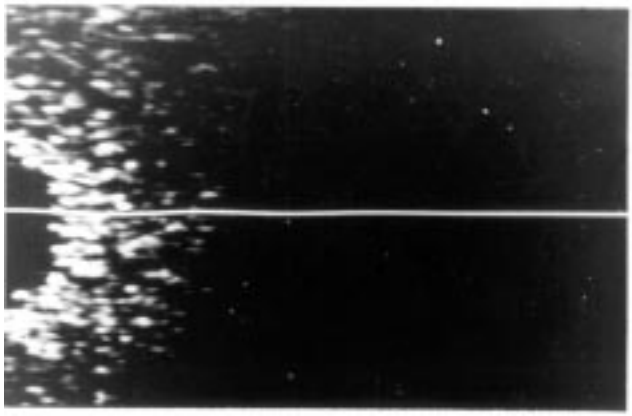

Figure 7. Photograph of the digitized image of the scattering spectrum.

A typical series of the angular spectra thus obtained presents the following pattern of the development of SD in time (Fig. 8). Until the moment $t \sim 1$ min from the onset of heating, the concentration distribution remains uniform and reflexes are absent. The onset of SD corresponds to the appearance of reflexes over the entire field of the television camera (Fig. 8b, $t = 1.3$ min). Then the scattered light practically disappears from the camera field because the SD structures become so large that their reflexes are blocked by the mask (Fig. 8c, $t = 1.5$ min).

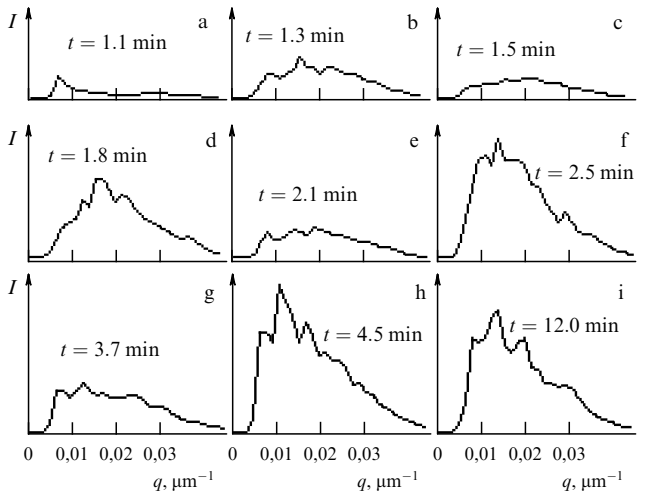

Figure 8. Dynamics of the angular spectrum of light scattering upon spinodal decomposition.

Spectrograms related to longer times distinctly demonstrate the periodicity of the process: the pattern typical of medium-scale structures of size 80–100 μm ($t = 1.8$ and 2.5 min) appears again, and is then replaced by the spectra typical of the large-scale structures hidden by the mask ($t = 2.1$ and 3.7 min). Finally, the scattering pattern becomes stable at $t \geqslant 4.5$ min, which corresponds to the termination of solution heating; and as a result, the system leaves the labile state. Therefore, the solution spends approximately 5 min in the labile region.

Figure 9 demonstrates the periodic time-dependent intensity of the radiation scattered by SD structures of size 100 μm. To exclude the temporal fluctuations of the television signal brightness, each ordinate was averaged over several successive spectrograms.

Therefore, SD distinctly demonstrates the 'return' effect, which is known in the physics of nonlinear systems (see, for example, Ref. [42]). This effect is indeed nonlinear because SD

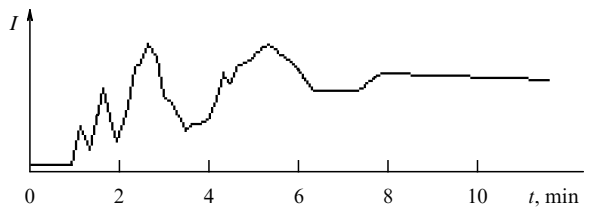

Figure 9. Time dependence of the intensity of a reflex from the structure of a fixed scale; the size of the structure is 100 μm.

is mainly determined by diffusion (monotonic in the linear regime) rather than wave processes. For its description, a theory should be developed which takes into account the nonlinear relation between the parameters of the problem (for example, the dependence of the relaxation times on concentration and the depth of quench into the labile region). Generally speaking, a nonlinear relation between parameters results in a nonlinear interaction between the concentration modes, whose superposition describes the fluctuation $u - u_0$, for a broad spectrum of the wave vectors $\mathbf{k}$ [see (1.2)], the spectrum being broadened with increasing ΔT. The consideration of such interactions presents a problem which has not been solved so far. In addition, the analysis given below does not take into account the wetting effects (we present below the theory for the volume case rather than for the near-surface case.) We also did not take into account the fact that SD develops during heating of the solution. (Notice that we considered the effect of wetting and nonstationary dependence on T in Ref. [37].) However, we found good agreement with experimental results within the framework of approximations made here.

2.3 Description of the dynamics of spinodal decomposition in the effective free energy approximation

It follows from the Gibbs–Duhem relation [41] that the free energy density for the homogeneous state at constant p and T takes the form

$$f = \mu_1 u_1 + \mu_2 u_2 - pv\,, \tag{2.1}$$

where N_1 and N_2 are the numbers of particles of two types, $u_1 = N_1/(N_1 + N_2)$ and $u_2 = N_2/(N_1 + N_2)$ are the concentrations, and v is the specific volume.

The energy functional has the general form

$$F = \int \mathrm{d}V \left[f(u) + K(u)(\operatorname{grad} u)^2 \right], \tag{2.2}$$

where $K(u)(\operatorname{grad} u)^2$ characterizes the energy of the 'concentration inhomogeneity' (hereafter we omit the subscript '1': $u_1 \equiv u$.) By varying (2.2) over concentration and using the equation of continuity for concentration

$$\frac{\partial u}{\partial t} + \operatorname{div} \mathbf{J} = 0\,, \tag{2.3}$$

and the expression for the concentration flow $\mathbf{J} = -L \operatorname{grad}(\mu_1 - \mu_2)$, we obtain, for the one-dimensional case, the equation

$$u_t = L\left(\frac{\partial f}{\partial u} - 2K u_{xx} \right)_{xx}. \tag{2.4}$$

We will use the Landau expansion for the free energy density:

$$f(u) = -\frac{a}{2} u^2 + \frac{d}{4} u^4\,. \tag{2.5}$$

Here, $a = \alpha(T - T_{\mathrm{cr}})/T_{\mathrm{cr}}$ is the main controlling parameter of the dynamic system. For a solution with a lower critical point, $a > 0$ in the supercritical region and $a < 0$ in the subcritical region. For $a > 0$, the linear solution of equation (2.4) becomes unstable. The dynamics of the system is determined by the competition between the instability, which results in an

unlimited growth of the linear solution, and the nonlinearity, which limits this growth.

Stationary ($u_t = 0$) solutions of equations (2.4) and (2.5) are determined by the first integral

$$\left(\frac{\partial u}{\partial x}\right)^2 = \frac{1}{K} f(u) + Au + B \equiv M(u)\,, \tag{2.6}$$

where A and B are the integration constants.

Integration of (2.6) gives three types of stationary solutions u_∞. The first type represents solitary solutions describing the phase-transition front. The second type represents solitary solutions having the form of a droplet of one of the equilibrium phases. The third type corresponds to spatially periodical solutions, which form the general type of stationary solutions:

$$u_\infty = \frac{u_2 - u_1 m\,\mathrm{sn}^2(k, \lambda x)}{1 - m\,\mathrm{sn}^2(k, \lambda x)}\,. \tag{2.7}$$

Here, u_i are the roots of the equation $M(u) = 0$ numbered in increasing order:

$$m = \frac{u_3 - u_2}{u_3 - u_1}\,, \qquad \lambda^2 = \frac{d}{8K}(u_4 - u_2)(u_3 - u_1)\,,$$

and $\mathrm{sn}\,(k, \lambda x)$ is the elliptic Jacobi's sine with modulus k:

$$k^2 = \frac{(u_3 - u_2)(u_4 - u_1)}{(u_4 - u_2)(u_3 - u_1)}\,.$$

Spatial concentration oscillations (2.7) occur between the values $u = u_2$ and $u = u_3$ with a period X equal to

$$X = \frac{2}{\lambda}\int_0^1 \mathrm{d}u\left[(1 - u^2)(1 - k^2u^2)\right]^{-1/2}. \tag{2.8}$$

To analyze the nonlinear nonstationary problem (2.4), we will use the 'slow period' method [36] assuming that the nonstationary solution has periodic spatial dependence (2.7) with time-dependent period $X(t)$. Let us represent $u(x, t)$ in the form

$$u = u_\infty\big(x, Z(\varepsilon_1 x, \varepsilon_2 t)\big)\,. \tag{2.9}$$

The 'test' function $Z(t)$ has the form $Z(t) = 1 - k^2(t)$. The vanishing of this function corresponds to a passage to the infinite period (2.8), i.e. the solution assumes that spatial periodicity is only possible in the nonstationary case. The nonstationary behaviour is manifested in the slow dependence $k(t)$; here, ε_1 and ε_2 are symbolic small parameters corresponding to the conditions of applicability of the 'slow period' approximation:

$$\left|\frac{\partial \ln Z}{\partial x}\right| \ll \frac{1}{X}\,, \left|\frac{\partial \ln Z}{\partial t}\right| \ll \frac{L}{X^2}\left|\frac{\partial f}{\partial(u^2)}\right|, \frac{LK}{X^4}\,. \tag{2.10}$$

By inserting (2.9) into (2.4), averaging the equation obtained over the spatial period X, taking into account (2.10), and expressing Z explicitly, we obtain the weakly nonlinear equation for Z near the phase boundary $\big(|Z| \ll 1\big)$:

$$\frac{\partial Z}{\partial t} = p_1\left(\frac{\partial Z}{\partial x}\right)^2 + \frac{p_2}{2}\frac{\partial^2 Z}{\partial x^2} - \frac{p_3}{3}\frac{\partial Z}{\partial x}\frac{\partial^3 Z}{\partial x^3} + p_4\frac{\partial^4 Z}{\partial x^4}\,, \tag{2.11}$$

where

$$\frac{p_1}{L} = (-a + 3du_1^2)\left(\frac{3}{4} + \frac{m}{1-m}\right) + 9du_1(u_2 - u_1) \times \left(1 + \frac{m}{1-m}\right)\frac{1}{1-m} + 6d(u_1 - u_2)^2\left(\frac{3}{8} + \frac{m}{1-m}\right)\frac{1}{(1-m)^2}\,,$$

$$\frac{p_2}{L} = (-a + 3du^2) + \frac{6du_1(u_2 - u_1)}{1-m} + \frac{3d(u_2 - u_1)^2}{(1-m)^2}\,,$$

$$\frac{p_3}{L} = 18K\left(\frac{3}{4} + \frac{m}{1-m}\right), \qquad \frac{p_4}{L} = -2K\,.$$

The introduction of the function $Z(t)$ is the main feature of analysis within a broad frequency spectrum of concentration waves. Note that for a narrow spectral packet (i.e. for shallow quenches into the labile region), one can use the expansion near the central frequency ω_0, which allows one to reduce the nonlinear equation (2.4) to the Landau – Ginzburg equation and to obtain the oscillatory regime for $u(x, t)$ in the initial stage of the development of nonlinearity; in the case of a broad frequency spectrum, an ensemble of possible oscillatory regimes should be introduced. It can be shown that this ensemble is specified by a set of parameters — the free constants A and B in the polynomial

$$M(u) = \frac{d}{4K}(u - u_0)^4 - \frac{a}{2K}(u - u_0)^2 + A(u - u_0) + B\,,$$

where u_0 is the initial concentration. By assuming that the 'asymmetry' coefficient A is a centrally-symmetric random function, we obtain $\bar{A} = 0$. One can show further that oscillatory regimes are possible for $0 \leqslant B \leqslant a^2/4Kd$. By assuming that B is a random variable over the interval $[0, a^2/4Kd]$ with average value $\bar{B} = a^2/8Kd$, we find the roots of the polynomial $M(u)$ that correspond to the average values computed over an ensemble of oscillatory regimes:

$$u_1 = -1.46\sqrt{\frac{a}{d}}\,, \qquad u_2 = -0.54\sqrt{\frac{a}{d}}\,,$$

$$u_3 = 0.54\sqrt{\frac{a}{d}}\,, \qquad u_4 = 1.46\sqrt{\frac{a}{d}}\,.$$

Knowing u_i, we successively find $m \approx 0.58$, $k^2 \approx 0.83$, $\lambda^2 \approx 3.42a/8K$, and $X \approx 4.7/\lambda \approx 1.46(2K/a)^{1/2}$. Then, we average (2.11) over an ensemble of possible oscillatory regimes; for this purpose, it is sufficient to recalculate the coefficients p_i, which are now explicitly related to the physical constants of equation (2.4):

$$p_1 = 20.6aL\,, \qquad p_2 = 12.5aL\,,$$

$$p_3 = 38.7KL\,, \qquad p_4 = -2KL\,.$$

We can see that the average values of the coefficients p_i are independent of the nonlinearity parameter d [see (2.5)]. This means that we have found the intermediate asymptotics over the nonlinearity parameter d for the space-time modulations:

for $d = 0$, modulations are impossible (for this reason, $d \neq 0$ in principle), but the average values of p_i are independent of d, suggesting the universality of the physical mechanism of the modulations.

The solution of equation (2.11) in the 'slow period' approximation (2.10) is represented by the sum $Z = Z_0 + \zeta$, where the 'background' function Z_0 is described by a linear diffusion equation

$$\frac{\partial Z_0}{\partial t} \approx p_2 \frac{\partial^2 Z_0}{\partial x^2} .$$

For a 'test' perturbation with a Gaussian profile

$$Z_0(0, x) = \frac{\mu}{(2\pi\Delta)^{1/2}} \exp\left(-\frac{x^2}{\Delta}\right),$$

where μ and $\Delta^{1/2}$ are the amplitude and spatial scale of the perturbation, we successively use approximation (2.10) and arrive at Airy's equation, whose solution takes the form

$$\zeta = c(p_3 qt)^{-1/3} \operatorname{Ai}\left[(x + p_1 qt)(p_3 qt)^{-1/3}\right],$$

where $\operatorname{Ai}(x, t)$ is the quasi-periodic Airy's function. The amplitude constant c is specified by the initial condition, the coefficient $q = 0.13\mu/\Delta$ being the decisive one. This solution yields the required result: the spatial period of the concentration distribution changes quasi-periodically in time and asymptotically tends to a stationary value (see Fig. 9). The quasi-period $\mathcal{T}$ slowly depends on the time:

$$\mathcal{T}_n = 7.7 y_n \left(\frac{p_3}{p_1^4}\right)^{1/3} \frac{\Delta^{7/6}}{\mu}, \tag{2.12}$$

where $y_1 = 2.30$, $y_2 = 2.70$, $y_3 = 4.05, \ldots$ are the zeros of Airy's function. The dependence of the quasi-period $\mathcal{T}_n$ on the material constants determining the phase transition $\left(p_{1,3} = p_{1,3}(a, d, K, L)\right)$ and boundary and initial conditions (via Δ and μ) was calculated approximately. We can now describe the condition of applicability (2.10) in the explicit form

$$X \ll \left(p_3^4 p_1^{-4} \Delta^{7/2}\right)^{1/9} . \tag{2.13}$$

Recall that the physical meaning of X is the average size of the spatial SD structure. Condition (2.13) means that the concentration fluctuations, whose scale is specified by the value of $\Delta^{1/2}$, should be large compared to the period X. Therefore, the above theory is valid for long-wavelength fluctuations, and SD is caused exactly by such fluctuations. Because $\Delta \sim l$, where l is the maximum size of a cell, condition (2.13) is valid, according to our estimates, over a finite spatial region near the spinodal.

It is important that the measurement of the period $\mathcal{T}$ along with the numerical refinement of the theory allows one to determine another combination of unknown constants of the phase transition model (2.5), namely, the period X of the spatial structure and the quasi-period $\mathcal{T}$ of the nonlinear concentration fluctuations. It is also interesting that the self-oscillation SD regime results from the nonlinearity of the problem itself and it is not necessarily related to the boundary effects (wetting).

3. Determination of the binodal and spinodal for laser irradiation of a solution undergoing stratification

Below, we describe an experiment on the photo-induced quenching of a phase separable solution into the metastable and labile regions. We also present a brief review of experimental methods for determining the binodal and spinodal.

3.1 Methods for determining phase curves in solutions undergoing stratification

Optical methods for determining binodals and spinodals of binary solutions are usually based on measuring parameters of the radiation scattered in a cell containing a solution of fixed concentration. Thus, the temperature at which the scattered light intensity sharply changes is taken as the binodal point. The spinodal temperature is also measured from light scattering. In accordance with the Ornstein–Zernike theory, the intensity of scattering by the concentration fluctuations of a binary mixture in the critical region has the form (see, for instance, Ref. [43]):

$$I \propto \left(\frac{u}{n}\frac{\mathrm{d}n}{\mathrm{d}u}\right)^2 \frac{T}{T_{\mathrm{cr}}}\left(\frac{T}{T_{\mathrm{cr}}} - 1 + \frac{1}{6} q^2 l_{\mathrm{c}}^2\right)^{-1}, \tag{3.1}$$

where T_{cr} is the critical temperature, u is the concentration of one of the components of the solution, n is the index of refraction, l_{c} is the correlation length of fluctuations u, $q = (4\pi/\lambda)\sin(\theta/2)$, and θ is the scattering angle. For a given concentration of the solution, it follows that

$$\lim_{q\to 0} \frac{1}{I} = \left(\frac{\partial \mu}{\partial u}\right)_{P,T} = b\left(\frac{T}{T_{\mathrm{cr}}} - 1\right)^{\gamma}, \tag{3.1a}$$

where γ is the critical index, and b is a constant. Furthermore, as follows from the Ornstein–Zernike theory, the width of the Rayleigh scattering line for critical mixtures is

$$\Delta\omega \approx D(T) q^2 \left[1 + \frac{1}{6} q^2 l_{\mathrm{c}}^2 \left(\frac{T}{T_{\mathrm{cr}}} - 1\right)^{-2}\right], \tag{3.2}$$

where $D(T)$ is the diffusion coefficient. Therefore, one finds

$$\lim_{q\to 0} \frac{\Delta\omega}{q^2} = D(T) = \alpha\left(\frac{\partial \mu}{\partial u}\right)_{P,T} = d\left(\frac{T}{T_{\mathrm{cr}}} - 1\right)^{\eta}, \tag{3.2a}$$

where η is another critical index, and α and d are the coefficients of proportionality. In Ref. [43], it was shown that since the condition $T_{\mathrm{cr}} \sim T_{\mathrm{s}}$ (where T_{s} is the spinodal temperature) should be met in the neighbourhood of T_{cr}, the substitution $T_{\mathrm{cr}} \to T_{\mathrm{s}}$ is possible in formulae (3.1a) and (3.2a). Then these formulae acquire the form

$$\lim_{q\to 0} \frac{1}{I} = \frac{b}{T_{\mathrm{cr}}^{\gamma}} (T - T_{\mathrm{s}})^{\gamma}$$

and

$$\lim_{q\to 0} \frac{\Delta\omega}{q^2} = \frac{d}{T_{\mathrm{cr}}^{\eta}} (T - T_{\mathrm{s}})^{\eta},$$

respectively. Therefore, the spinodal points can be obtained by the extrapolation of the dependences $1/I = f_1(T)$ and $\Delta\omega/q^2 = f_2(T)$ to the zero value of q at a fixed concentration. Since the validity of such an extrapolation away from T_{cr}

is not rigorously theoretically substantiated, this method is only efficient near the critical temperature. Notice that for $T \sim T_{cr}$ the time of relaxation to the equilibrium state is long and the solution may be in the labile state for a sufficient time to perform the required measurements.

An alternative method for measuring binodal and spinodal positions in a solution undergoing stratification was suggested in Ref. [30]. The homogeneous state of the solution in the metastable and labile regions was maintained by vigorous mixing. In the experiment, the temperature dependence of the heat capacity C_V of the mixture was measured at the fixed initial concentration of the solution. The dependence $C_V(T)$ exhibits two singularities at temperatures T_1 and T_2 ($T_1 > T_2$). The point T_1 corresponds to the binodal, while the point T_2 does that to the spinodal of the solution at a given concentration. The height of the C_V peaks at points T_1 and T_2 increases with increasing mixing frequency. The anomalous response of the system at temperature T_2 is explained in Ref. [30] by the effect of 'pulling behind the spinodal' due to vigorous mixing. Thus, in Ref. [30] not only a labile state of the phase separable system was achieved but also the position of the boundary of the labile region was determined.

In the experiment described below in Section 3.3, the mechanism of solution mixing is also realized. The mixing occurs in a thin cell due to turbulent flows caused by optical (laser-induced) cavitation. It is also shown that in the absence of optical cavitation a vital mechanism of the local equilibrium shift is the photo-induced barodiffusion of molecules in the region of the laser spot. The theoretical analysis of photo-induced processes in the field of powerful laser pulses is presented below.

3.2 Local photo-induced stratification

Consider the behaviour of an isotropic binary solution in which a monochromatic wave with frequency ω and electric field strength

$$\mathbf{E} = \frac{1}{2}\left[\mathbf{x}E(x,y,t)\exp(-\mathrm{i}\omega t + \mathrm{i}kz) + \text{c.c.}\right]$$

is propagating along the z-axis. The dynamics of the solution is described by a system of equations [4, 39], which includes the equations of continuity

$$\frac{\partial\rho}{\partial t} + \boldsymbol{\nabla}\cdot(\rho\mathbf{v}) = 0\,, \tag{3.3}$$

of production of entropy S

$$\rho T\left[\frac{\partial S}{\partial t} + (\mathbf{v}\cdot\boldsymbol{\nabla})S\right] = -\boldsymbol{\nabla}\cdot(\mathbf{q} - \mu\mathbf{i}) - (\mathbf{i}\cdot\boldsymbol{\nabla})\mu + \left(\frac{4\eta}{3} + \zeta\right)(\boldsymbol{\nabla}\cdot\mathbf{v})^2 + \frac{cn\delta\mathbf{E}^2}{4\pi}\,, \tag{3.4}$$

of conservation of mass for each of the components

$$\frac{\partial u}{\partial t} + (\mathbf{v}\cdot\boldsymbol{\nabla})u = -(\boldsymbol{\nabla}\cdot\mathbf{i})\,, \tag{3.5}$$

and of conservation of momentum (the Navier–Stokes equation)

$$\rho\left[\frac{\partial\mathbf{v}}{\partial t} + (\mathbf{v}\cdot\boldsymbol{\nabla})\mathbf{v}\right] + \boldsymbol{\nabla}P - \left(\frac{4\eta}{3} + \zeta\right)\boldsymbol{\nabla}\cdot(\boldsymbol{\nabla}\cdot\mathbf{v}) = \rho\,\frac{\partial\varepsilon}{\partial\rho}\,\boldsymbol{\nabla}\cdot\frac{\mathbf{E}^2}{8\pi}\,. \tag{3.6}$$

Here, ρ, P, δ, and ε are the density, pressure, absorption coefficient, and permittivity of the solution; η and ζ are the coefficients of dynamic and shear viscosity. The last term in the right-hand side of equation (3.4) determines the heat flow caused by absorption of light in the liquid. The right-hand side of equation (3.6) defines the electrostriction force in an inhomogeneous electric field. In (3.3)–(3.6), the averaging over the period of the light wave has already been performed: the thermodynamic quantities change for a time that far exceeds its period.

Under the action of the light wave, the system becomes nonequilibrium and the diffusive heat $\mathbf{q}$ and mass $\mathbf{i}$ flows appear, which tend to return the solution to thermodynamic equilibrium. The viscous friction caused by the irreversible momentum transfer also produces entropy [the third term on the right of Eqn (3.4)]. Assuming that deviations from the equilibrium state are small, we expand $\mathbf{q}$ and $\mathbf{i}$ in a power series of gradients of the chemical potential and temperature [39]:

$$\mathbf{i} = L_{11}\boldsymbol{\nabla}\mu - L_{12}\boldsymbol{\nabla}T\,,$$
$$\mathbf{q} - \mu\mathbf{i} = -TL_{12}\boldsymbol{\nabla}\mu - L_{22}\boldsymbol{\nabla}T\,. \tag{3.7}$$

Here, L_{ij} are the Onsager coefficients, which determine the rate of establishment of thermodynamic equilibrium. In particular, the coefficient of kinetic mobility L_{11} specifies the rate of mass diffusion. The system of equations (3.3)–(3.7) is closed via the equation of state.

Let us linearize the system (3.3)–(3.7) over small deviations of the thermodynamic variables from their equilibrium values. These deviations will be denoted as S, T, ρ, P, and u; the subscript '0' corresponds to the equilibrium values of these parameters. Using the set of thermodynamic variables T, P, and u, we arrive at the closed system of equations for the dimensionless thermodynamic variables u, $\Theta = T/T_0$, and $p = P/P_0$:

$$\frac{\partial u}{\partial t} = D(\nabla^2 u + k_T\nabla^2\Theta + k_P\nabla^2 p - k_E\nabla^2 I)\,, \tag{3.8}$$

$$\frac{\partial\Theta}{\partial t} - \frac{k_T}{k_E}\left(\frac{\partial\varepsilon}{\partial u}\right)_{P,T}\frac{\partial u}{\partial t} = \chi\nabla^2\Theta + b\beta_P\,\frac{\partial p}{\partial t} - T_0\left(\frac{\partial\varepsilon}{\partial T}\right)_{P,u}\frac{\partial I}{\partial t} + \frac{I}{\tau_\delta}\,, \tag{3.9}$$

$$\frac{\partial}{\partial t}\left(\frac{\partial}{\partial t} - \nu\nabla^2\right)\left(\frac{\beta_u}{\beta_P}\,u + \frac{\beta_T}{\beta_P}\,\Theta + p\right) - u_T^2\nabla^2 p = -\frac{u_T^2}{b}\,\rho_0\left(\frac{\partial\varepsilon}{\partial\rho}\right)_{T,u}\nabla^2 I\,. \tag{3.10}$$

Here, standard notations are introduced for the isobaric heat capacity c_P, the kinematic viscosity $\nu = (4\eta/3 + \zeta)/\rho$, the diffusion coefficients

$$D = \frac{L_{11}}{\rho_0}\left(\frac{\partial\mu}{\partial u}\right)_{P,T}$$

and the thermal conductivity

$$\chi = \left(L_{22} - \frac{L_{12}^2 T_0}{L_{11}}\right)\frac{1}{\rho_0 c_P}\,.$$

Furthermore, $I = E^2/8\pi\rho_0 c_P T_0$ is the dimensionless light intensity;

$$k_T = T_0\left[\left(\frac{\partial\mu}{\partial T}\right)_{u,P} + \frac{L_{12}}{L_{11}}\right]\left[\left(\frac{\partial\mu}{\partial u}\right)_{P,T}\right]^{-1}$$

is the thermal diffusion ratio;

$$k_P = \frac{P_0\beta_u}{\rho_0}\left[\left(\frac{\partial\mu}{\partial u}\right)_{P,T}\right]^{-1}$$

is the barodiffusion ratio; v_T is the isothermal sound velocity, with $v_T^2 = P_0/\rho_0\beta_P$, and $\tau_\delta = 2/\delta cn$ is the time of optical dissipation. Also, the dimensionless parameters

$$k_E = \left(\frac{\partial\varepsilon}{\partial u}\right)_{P,T} c_P T_0\left[\left(\frac{\partial\mu}{\partial u}\right)_{P,T}\right]^{-1},$$

$$b = \frac{P_0}{\rho_0 c_P T_0}, \qquad \beta_u = \rho_0\left[\frac{\partial(1/\rho)}{\partial u}\right]_{T,P},$$

$$\beta_T = \rho_0 T_0\left[\frac{\partial(1/\rho)}{\partial T}\right]_{u,P}, \qquad \beta_P = P_0\rho_0\left[\frac{\partial(1/\rho)}{\partial P}\right]_{u,T}$$

are introduced.

The system of equations (3.8)–(3.10) allows one to describe consistently the photo-induced processes in a binary solution; it is valid with an accuracy to the second spatial derivatives of u, p, and Θ; the products of the light intensity by the kinetic parameters (diffusion and thermal diffusion coefficients, etc.) are assumed to be negligibly small. The times of perturbation development are determined by the following set of parameters in (3.8)–(3.10), which are typical of many solutions: $D \sim 10^{-6}$ cm^2 s^{-1}, $\chi \sim 10^{-3}$ cm^2 s^{-1}, $k_T \sim k_P \sim 10^{-1}-1$, $k_E \sim 10^2-10^4$, $\tau_\delta \sim 10^{-8}$ s, $v_T \sim 10^5$ cm s^{-1}, $b \sim 10^{-3}-10^{-4}$, $\beta_u \sim \beta_T \sim 10^{-2}-10^{-1}$, and $\beta_P \sim 10^{-4}-10^{-5}$. The substitution of expressions for $\partial u/\partial t$ and $\partial\Theta/\partial t$ from (3.8) and (3.9) into (3.10) brings, in the above approximations, this equation to the form

$$\frac{\partial^2 p}{\partial t^2} + v_{\text{eff}}\nabla^2\frac{\partial p}{\partial t} - v^2\nabla^2 p = -c_P T_0\rho_0\left(\frac{\partial\varepsilon}{\partial\rho}\right)_{T,u}\nabla^2 I - \frac{\beta_T\rho_0 v^2}{P_0}\left[T_0\left(\frac{\partial\varepsilon}{\partial T}\right)_{P,u}\frac{\partial^2 I}{\partial t^2} - \frac{1}{\tau_\delta}\frac{\partial I}{\partial t}\right], \tag{3.11}$$

where $v^2 = v_T^2/(1 + b\beta_T^2/\beta_P)$ is the square of the adiabatic velocity of sound, and $v_{\text{eff}} = v + \chi(v_T^2/v^2 - 1) + (L_{11}/\rho_0)v^2\beta_u^2$ is the effective viscosity. Therefore, in these approximations, the perturbation of pressure is not related to variations of u and Θ in the light field. The role of diffusion and thermal conductivity is reduced to an increase in the rate of pressure relaxation to the equilibrium value (resulting in a broadening of the Brillouin scattering line). In this case, the contribution of the diffusion is proportional to the mobility coefficient L_{11}, which permits a direct measurement of the coefficient from the width of the line of spontaneous scattering by concentration fluctuations [44]. The terms in the right-hand part of Eqn (3.11) correspond to three mechanisms of light scattering by acoustic perturbations: electrostriction, the electrocaloric effect, and light absorption.

We shall further assume that the length of light propagation (the length d of a cell with the solution) is not sufficient for the development of stimulated scattering ($Gd \ll 30$, where G is the increment of stimulated scattering [45]). Just this situation is realized in the experiment with a thin cell described below, where the light beam intensity can be considered constant along its propagation direction. For this reason, the pressure, concentration, and temperature are independent of z. The photo-induced perturbations propagate only in the transverse direction and the problem becomes two-dimensional, the establishment time of the transverse pressure distribution being of the order of R^2/v_{eff}, where R is the laser beam radius. Under typical conditions ($R \sim 10^{-1}$ cm), this time is hundreds of milliseconds. Therefore, a nanosecond pulse of duration τ can be treated as a delta function:

$$I(r,t) = \frac{W}{\tau}\exp\left(-\frac{r^2}{R^2}\right)\delta\left(\frac{t}{\tau}\right), \tag{3.12}$$

where W is the light energy flux density, and $r^2 = x^2 + y^2$ is a coordinate in the plane perpendicular to the beam. By substituting (3.12) into (3.11), we can calculate the space-time evolution of pressure. For the times $t > \max(\tau, R/v, \tau_\delta)$, equation (3.11) can be solved using the integral Fourier–Bessel transformation. Its solution shows that, for the above typical values of parameters, heating of the mixture caused by light absorption is the major factor at $t > \tau_\delta$:

$$p \simeq \frac{\rho_0\beta_T R^2 W}{2P_0\tau_\delta t^2}, \qquad \nabla^2 p \simeq \frac{3\rho_0\beta_T R^2 W}{P_0\tau_\delta v^2 t^4}. \tag{3.13}$$

Integrating equations (3.8) and (3.9) with respect to time

$$\Delta\Theta = \int \mathrm{d}t\,\frac{\partial\Theta}{\partial t}, \qquad \Delta u = \int \mathrm{d}t\,\frac{\partial u}{\partial t} \tag{3.14}$$

gives the photo-induced variations of temperature and concentration. Taking into account the estimates $\chi\tau/R^2 \sim 10^{-6}$, $\tau k_T/\tau_\delta k_E \sim 10^{-2}-10^{-4}$ for $\tau \sim 10^{-8}$ s, $D\tau/R^2 \sim 10^{-8}$, and

$$\frac{k_T}{k_E}\left(\frac{\partial\varepsilon}{\partial u}\right)_{P,T} \sim 10^{-2}-10^{-4}, \qquad \frac{D}{\chi}\frac{k_T}{k_E}\left(\frac{\partial\varepsilon}{\partial u}\right)_{P,T} \sim 10^{-4}-10^{-6}$$

we obtain

$$\Delta\Theta = \frac{W}{\tau_\delta}. \tag{3.15}$$

In order to calculate Δu, one should know the time dependence of the pressure in the solution for the times $t \leqslant \tau$ as well; its maximum can be evaluated as $(\rho_0\partial\varepsilon/\partial\rho)E^2(t)/16\pi$. Taking into account (3.13), we finally obtain that the steady-state concentration is mainly determined by barodiffusion:

$$\Delta u \simeq Dk_P\frac{\rho_0 v^2}{P_0}\beta_T\frac{\mathcal{E}\delta}{v^4\tau^3\rho_0 c_P T_0}, \tag{3.16}$$

where $\mathcal{E} = \tau cnE^2R^2/8\pi$ is the laser pulse energy.

The estimate (3.16) gives $\Delta u \sim 10^{-3}$ for typical values of the parameters of phase separable solutions, a laser pulse energy of the order of 10 mJ, and an absorption coefficient 10^{-2} cm^{-1}. Thus, under the action of heating and barodiffusion caused by laser irradiation the solution is quenched into

the new phase state $(u_0 + \Delta u, T_0 + \Delta T)$, its shift relative to the initial (u_0, T_0) state being determined by Eqns (3.15) and (3.16). For the (u_0, T_0) states lying in the stable region near the binodal, this shift can provide a local (within the light spot) quasi-equilibrium (the lifetime of the new state is $\tau_n \sim R^2/D \gg \tau$ for nanosecond pulses) solution stratification — quenching to the metastable region. This causes the 'response' to the laser action observed in experiments. The effect is more pronounced if $u_0 \lesssim 10^{-2} - 10^{-1}$. The optical mechanism of u variation is efficient if the binodal $T_b(u)$ is asymmetric, which is typical of mixtures of azines with intermolecular hydrogen bonds N...HO (see, for example, Fig. 4).

A solution in the metastable (u, T) state undergoes stratification during the time of perturbation relaxation $\tau_n \sim R^2/D$ into two phases (u_L, T) and (u_R, T) lying at the left and right branches of the binodal, respectively. This process proceeds via the growth of spontaneous nuclei of the conjugate phase that corresponds to the (u_L, T) phase in Fig. 10. It is natural to specify the main (u_R, T) phase by the condition $|u_R - u_0| < |u_L - u_0|$. The work of formation of spherical nuclei of radius a is minimum at $a = a_{cr}$ [46]:

$$a_{cr} = \frac{2\sigma}{\rho_0 \Delta\mu}\,, \tag{3.17}$$

where $\Delta\mu = \mu_R - \mu_L$, and σ is the interface tension at the boundary between the two phases. The nuclei of radius $a < a_{cr}$ are dissolving, while the nuclei of radius $a > a_{cr}$ should grow according to energy considerations. The critical radius a_{cr} (3.17) has a singularity at the binodal: for $\Delta\mu = 0$, $a_{cr} \to \infty$ in the absence of the light field. The photo-induced barodiffusion qualitatively changes the dependence of the critical radius a_{cr} on u and T:

$$\frac{2\sigma}{\rho_0 a_{cr}} = \Delta\mu_0 + \frac{\partial\mu}{\partial u}\,\Delta u + \frac{\partial\mu}{\partial T}\,\Delta T\,, \tag{3.18}$$

where $\Delta\mu_0$ is the difference between the chemical potentials of the two phases in the absence of the field. It follows from the above estimates that the 'light absorption → heating of the medium → thermal expansion → barodiffusion' process makes the main contribution to Eqn (3.18). Taking this into account, the temperature dependence of the radius of a stable nucleus, at a given concentration, can be written in the form

$$a_{cr}(T) \simeq 2\sigma(T)\left[\rho_0\left(\Delta\mu_0 + \frac{\beta_u \beta_T D \delta\mathcal{E}}{\rho_0 c_P T_0 v^2 \tau^3}\right)\right]^{-1}. \tag{3.19}$$

Owing to the second term in the parentheses in Eqn (3.19) responsible for the laser action, the condition

$$|\Delta\mu_0| \lesssim \frac{\beta_u \beta_T D \delta\mathcal{E}}{\rho_0 c_P T_0 v^2 \tau^3}\,.$$

can be met for a solution in the stable region (where it is assumed that $\Delta\mu < 0$) near the binodal. For this reason, $a_{cr}(T) < \infty$, i.e. the solution is quenched into the metastable region. Because of this, we speak of photo-induced stratification phase transition.

In addition, it is assumed [47] that the coefficient of interface tension σ approaches zero at $T \to T_s$, i.e. nuclei are formed at the spinodal without an energy barrier. Therefore, it follows from (3.19) that a_{cr} has singularities near the binodal and spinodal. These singularities should also appear in the dependence $S(T)$ of the average area occupied by nuclei in an arbitrary plane section of a cell with the solution [48, 49]. The kinetic theory of solution stratification in a laser field describing the growth, segregation, and dissolving of nuclei of the conjugate phase upon photo-induced quenching into metastable and labile regions is a subject for a separate paper. In conclusion, note that the dependence (3.19) substantially depends on the sign of the barodiffusion parameter β_u, which takes the simple form

$$\beta_u = \frac{m_2 - m_1}{m_1 + (m_2 - m_1)u}\,, \tag{3.20}$$

where $m_{1,2}$ are the molecular masses of the components, i.e. the barodiffusion parameter is positive for the light component $(m_1 < m_2)$ and negative for the heavy component $(m_1 > m_2)$. For this reason, heavy molecules are pulled into the region of elevated pressure. Notice that the barodiffusion mechanism of concentration variation is suppressed in mixtures of molecules with close masses.

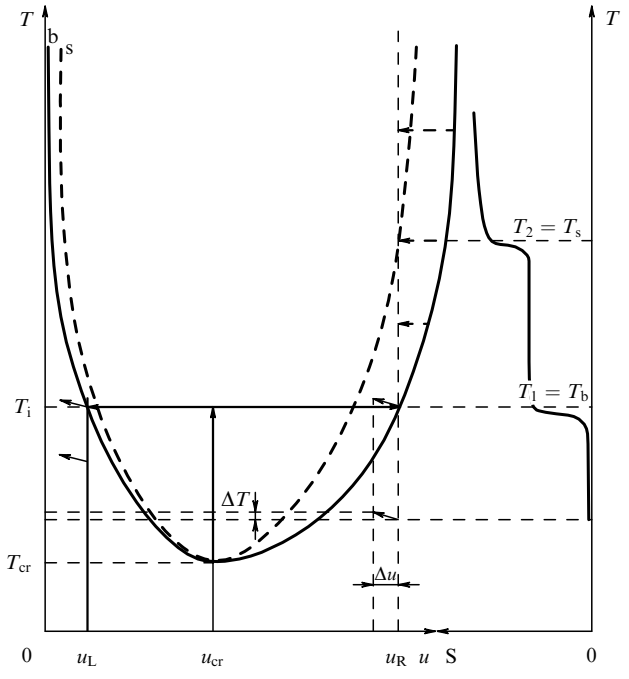

Figure 10. Phase diagram illustrating the optical method for determining the positions of the binodal and spinodal; the inclined and dashed horizontal arrows correspond to the changes caused by photo-induced barodiffusion and cavitation mixing, respectively.

3.3 Experimental realization of the optical method for determining the binodal and spinodal

Experiments on photo-induced quenching into the metastable and labile regions were performed with an associated water solution of TMP [48, 49]. The response being measured was the amount of the conjugate phase detected in the irradiated region due to local variation in the equilibrium concentration. In the experiment (Fig. 11), a pulsed-periodic Q-switched Nd^{3+}:YAG laser (*1*) was used ($f = 10$ Hz, $\lambda = 1.06$ μm, pulse duration $\tau = 15$ ns). The laser pulse energy and peak intensity were $\mathcal{E} = 20$ mJ and $I_p = 50$ mW cm^{-2}, respectively. The solution was irradiated

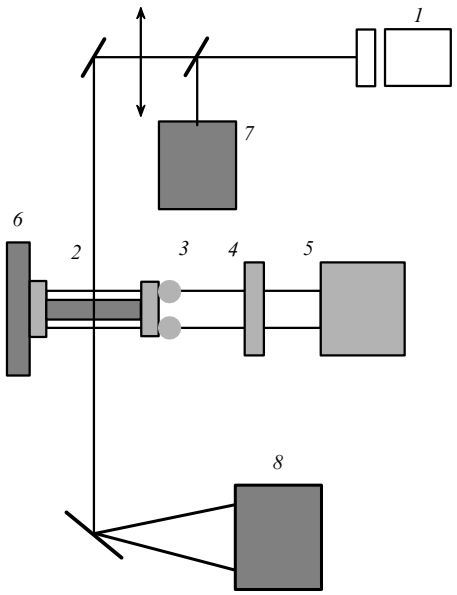

Figure 11. Schematic of the experimental setup: (*1*) Nd^{3+} : YAG laser; (*2*) cell containing solution; (*3*) x-y table; (*4*) CAMAC module; (*5*) IBM PC; (*6*) thermostat; (*7*) an IMO-2N power meter; (*8*) microscope.

in a thin-layer cell *2* (the gap between the windows is $d = 25$ μm). Hydrodynamic processes in such a cell are suppressed (see Section 2.1). The laser beam was focused on the cell with a lens; however, the focusing was not sharp in order to avoid an optical breakdown (a laser spark). The cell was connected with a fluid thermostat *6*, which served to control the solution temperature with an accuracy of 0.1 K. The cell was mounted on an $x - y$ table *3*, which moved it across the laser beam with the help of ShDR-711 step motors controlled by a computer *5* via a CAMAC module *4*.

To obtain a solution with the specified concentration u_R of water, the pristine mixture of TMP and water with concentration u_{cr} was poured into a vertical capillary 5 mm in diameter and was settled here for twenty-four hours at some initial temperature $T = T_i > T_{cr}$. This resulted in stratification of the solution into light and heavy fractions whose concentrations were determined by the left u_L (for the light fraction) and right u_R (for the heavy fraction) points of intersection of the straight line $T = T_i$ with the binodal (see Fig. 10). One can see from Fig. 10 that the concentration of heavy TMP molecules in the light fraction is always higher than in the heavy fraction. All our experimental data will refer to concentrations u_R. The heavy (main) fraction was placed in a thin-layer cell whose windows were kept at a temperature $T < T_i$. The cell was located in the field of the microscope objective and was illuminated by laser pulses. A microscope *8* was used to observe the appearance of microdroplets of the light (conjugate) fraction in the solution.

At the binodal temperature $T_b(u_R)$, a uniform (over the cell area) background of microdroplets $\sim 1-5$ μm in size was observed in the microscope field (Fig. 12a; the photograph was obtained in the microscope dark field.) Upon lowering temperature by a degree, the microdroplets disappeared. The density of microdroplets and their size increased with increasing cell temperature above T_i. Just this fact confirms that the temperature T_i of the solution settling in a cell coincides with the binodal temperature $T_b(u_R)$.

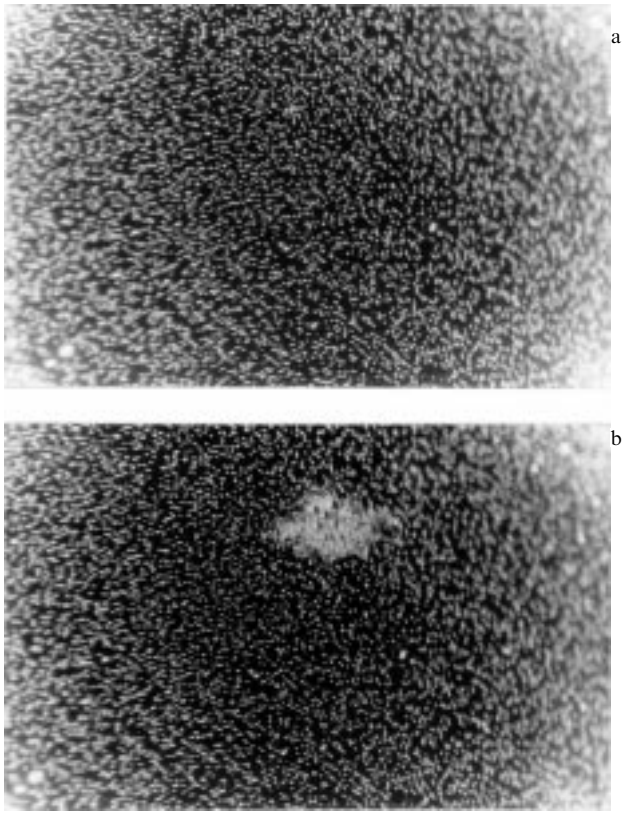

Figure 12. Photo-induced segregation of the conjugate phase in a mixture of TMP and water. A general view of microdroplets of the light fraction inside the heavy fraction (a) before and (b) after irradiation ('shot') by the laser pulse. The size of the 'fogginess' consisting of microdroplets of the conjugate phase is ~ 100 μm.

A cell was illuminated by a single pulse separated with the help of an electromechanical shutter from the laser pulse train. Figure 12b shows the response of the solution to the pulse passing through the cell at temperature $T > T_i$. Inside the laser spot, a 'fogginess' is formed consisting of microdroplets of the conjugate phase with substantially higher density. The lifetime of the fogginess, shown on the photograph, is about 1 min. The first responses (with the lifetimes of order several seconds) appeared at a temperature $1-1.5$ K below $T_i = T_b(u_R)$, when the background of microdroplets of the conjugate phase was still absent. This confirms the theoretical conclusion made in Section 3.2 that laser irradiation can stimulate nucleation of the conjugate phase at $T \lesssim T_b$, resulting in a brief (limited by the time of conventional diffusion) quench into the metastable region. At the same time, the photo-induced segregation of the conjugate phase was not observed upon laser irradiation of the light fraction of the solution [the (u_L, T) state corresponding to the intersection of the temperature straight line T with the left branch of the binodal], even when the radiation intensity was increased by an order of magnitude. Indeed, because barodiffusion shifts heavier molecules to the region of elevated pressure, whereas lighter molecules are ejected from this region, photo-induced barodiffusion should stabilize the (u_L, T)-state. This is illustrated by the arrow in Fig. 10, which is directed towards the stable region.

The absence of the effect for the left branch of the binodal suggests that heating does not play a key role in our case (indeed, if the photo-induced solution stratification had taken

place exclusively as a result of laser heating, the arrows in Fig. 10 would have been vertical and the effect would have been observed for both binodal branches.) In addition, the effect was not observed in phase separable solutions with identical molecular masses (as indeed should be in the case for barodiffusion.) This has been demonstrated in experiments on the laser irradiation of heavy and light fractions of solutions of methyl cyclohexane (molecular mass $M = 98$ amu) and furfural ($M = 96$ amu) and also of isoamyl alcohol ($M = 88$ amu) and glycerol ($M = 92$ amu). Therefore, the response of the heavy fraction of the water solution of TMP in the stable region near the binodal to the laser irradiation is really caused by photo-induced barodiffusion. To our knowledge, this is the first observation of photo-induced barodiffusion in a liquid.

The area S of the fogginess can serve as a natural quantitative characteristic of the solution response to the laser action (Fig. 12b). Because of the irregular shape of the fogginess and its blurred boundary, the relative error $\Delta S/S$ of measuring S for a single laser pulse is quite large. The measuring accuracy was improved by irradiating a cell, kept at a certain temperature, by a series of 250 laser pulses. Each subsequent pulse fell on a different site of the cell — during 10-s pauses, the cell was shifted across the laser beam by 1 – 2 mm with the help of the $x - y$ table. The averaging of areas S over a set of 250 independent values resulted in a decrease in the measuring error $\left(\langle \Delta S^2 \rangle\right)^{1/2}/\langle S \rangle$ to 5%.

After the termination of a series of 250 pulses and complete relaxation of the fogginess, the temperature T of the cell was increased and the procedure of measuring $S(T)$ was repeated. Thus, we determined the temperature dependence of the fogginess area $S = S(T)$ for each initial concentration u_R of the solution. The family of five such dependences is shown in Fig. 13a – e. In all five cases, the first series of laser pulses began after the cell was cooled down to a temperature $T < T_i(u_R)$ (when droplets of the light fraction were absent); the temperature step of measurements was 0.5 K. One can see from Fig. 13 that, beginning from some temperature, the function $S(T)$ increases and flattens out at $T_1 = T_b(u_R)$; in this case, as was mentioned above, $S(T)$ starts to increase at a temperature approximately 1 K below T_b. By measuring the temperature T_1 of the plateau reaching, we could independently determine the binodal temperature T_b. The function $S(T)$ has no additional singularities up to a temperature T_2, where it exhibits a jump; then it flattens out again. Because, as follows from the above plots, temperatures T_2 and T_1 come close to each other and tend to T_{cr} at $u_R \to u_{cr}$, it is reasonable to relate T_2 to the spinodal temperature $T_s(u_R)$. Therefore, the dependence $S(T)$ confirms the theoretical conclusion in Section 3.2 [see Eqn (3.19)] about the existence of singularities of the dependence $a_{cr}(T)$ at the binodal and spinodal points. Notice that we observed sporadic photo-induced cavitation in the solution at $T > T_b$: a cavitation bubble appeared in the region of the laser spot (Fig. 14).

The experimental points $T_b(u_R)$ and $T_s(u_R)$ are presented in Fig. 15. The solid curve corresponds to the binodal of the water solution of TMP taken from handbook [38] (see also Fig. 14). One can see that the binodal fits the experimental values of $T_b(u_R)$ rather well, i.e. these points belong to the binodal.

We suggest the following mechanism for the solution's response to the laser action on reaching the temperature T_s. As shown in Section 2.1, a convective counterflow in a cell is

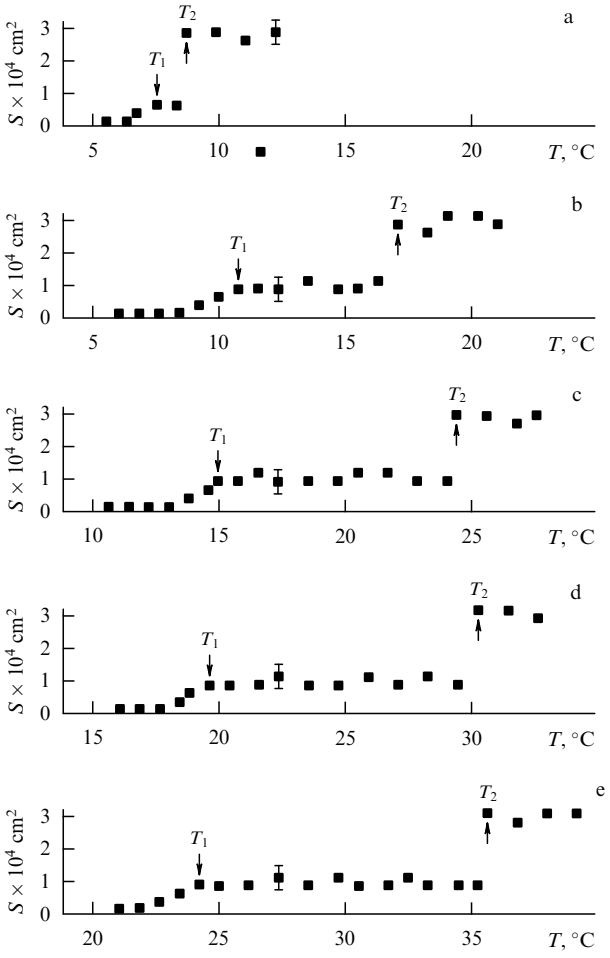

Figure 13. Experimental dependence of the cross section $S(T)$ of droplets of the conjugate phase in the irradiated solution at (a) $T_i = 7\,^\circ$C ($u_R = 2$ mol.% of TMP), (b) $T_i = 11\,^\circ$C ($u_R = 1$ mol.% of TMP), (c) $T_i = 15\,^\circ$C ($u_R = 0.85$ mol.% of TMP), (d) $T_i = 19\,^\circ$C ($u_R = 0.7$ mol.% of TMP), and (e) $T_i = 23\,^\circ$C ($u_R = 0.5$ mol.% of TMP).

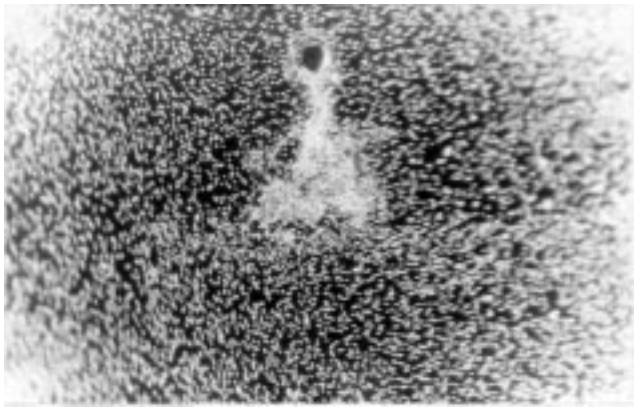

Figure 14. Response to laser irradiation of a water solution of TMP upon excitation of optical cavitation.

suppressed and the conjugate phase is dispersed inside the main phase in the form of tiny droplets (Fig. 12a), i.e. the concentration distribution is inhomogeneous. Let us choose a region in this stratified solution inside the laser spot that

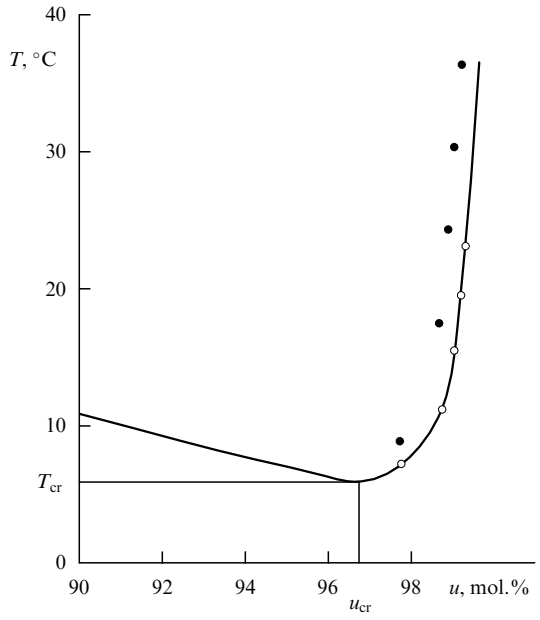

Figure 15. Part of the phase diagram of the water solution of TMP. The solid curve is the binodal [38]. The open circles are experimental points of the binodal $T_b(u_R)$; the dark circles are experimental points of the spinodal $T_s(u_R)$; u_R is the molecular concentration of TMP.

contains rather many droplets of the conjugate phase. The average concentration of molecules of some type (for certainty, TMP molecules) in this region is defined as $\bar{u}_t = N_t/(N_t + N_w)$, where N_t and N_w are the concentrations of the TMP and water molecules in this region, respectively. Notice that $\bar{u}_t$ is not a real concentration of the mixture in the chosen region, because the concentration in each point of this region is determined by the binodal abscissae and corresponds to the light or heavy fraction. However, it is clear that $\bar{u}_t \approx u_R$, where u_R is the initial concentration of the TMP molecules, which depends on the temperature T_i at which this heavy fraction was obtained (see Fig. 10). Let us assume that the temperature T controlled by a thermostat is such that the point (u_R, T) lies on the spinodal, i.e. $T = T_s$. To obtain the labile state, we should mix the solution that underwent stratification, keeping it at a temperature T_s. As a result, the concentration distribution over the separated region becomes quasi-homogeneous, i.e. the average concentration $\bar{u}_t \approx u_R$ corresponds to the physical concentration, and the (u_R, T_s)-state is experimentally realized. This is illustrated by the dashed horizontal arrow in Fig. 10.

Mixing can occur due to hydrodynamic eddy flows caused by the optical (photo-induced) cavitation — the formation of a macroscopic bubble (see Fig. 14). In our experiments, the sporadic cavitation regime was realized, cavitation not being produced by every laser pulse (the excitation of various regimes of optical cavitation in transparent liquids is described in Ref. [50]; we considered this phenomenon in phase separable polar liquids in Ref. [51].) It is known [52] that upon optical cavitation of a low-viscosity liquid near a rigid wall, eddy flows do appear in the vicinity of a bubble. Notice that in the case of optical cavitation, a weak effect of photo-induced barodiffusion (which destroys the quasi-homogeneous concentration distribution, i.e. hinders mixing) can be neglected. This is indirectly indicated by a regular segregation of the conjugate phase in a mixture of methyl cyclohexane and furfural and by the absence of this effect in a mixture of isoamyl alcohol and glycerol during optical cavitation (recall that barodiffusion in these liquids is prohibited.) The absence of the effect in the latter case is explained by the fact that one of the components is glycerol, so that the solution viscosity is too high for the excitation of hydrodynamic flows. In order to find the spinodal position more exactly, the region of mixing should be large and contain a sufficient number of droplets of the conjugate phase (in this case, the average concentration in the region of mixing will be close to the initial value.) This can be achieved in the case of a low-viscosity liquid. Returning to a mixture of TMP and water, note that in the absence of cavitation at $T > T_b$ the response to laser action is caused by photo-induced barodiffusion (it is this situation that is depicted in the photograph in Fig. 12b: there is no cavitation bubble in the region of segregated, conjugated phase.)

The experimental function $S(T)$ in Fig. 13 also allows one to obtain information on the temperature dependence of the coefficient σ in Eqn (3.19) in the metastable region, which is *a priori* unknown. The nonmonotonic dependence of $S(T)$ (the presence of the second jump) suggests, in particular, that $\sigma(T)$ decreases upon approaching the spinodal more rapidly than linearly.

Finally, note that our method for finding the spinodal is less efficient near the critical point because it requires stabilization of the temperature inside a cell and a capillary with an accuracy of 0.01 K, which is hard to achieve with the help of a normal thermostat. In addition, near the critical point the results will be also distorted by the thermal action of the laser pulse [see Eqn (3.15)] and the heat release due to the formation of a cavitation bubble and mixing. Therefore, our method is efficient for determining the spinodal position using a standard thermostatic control in the temperature range $1\ \mathrm{K} \lesssim T - T_{cr} \lesssim 10\ \mathrm{K}$, where the use of extrapolation procedures is hindered.

4. Conclusions

The observation of the spinodal decomposition of a phase separable binary mixture of 2,4,6-trimethylpyridine and water upon suppression of convective phase separation shows that the scales of spatial structures formed upon spinodal decomposition in the labile region undergo quasi-periodic variations in time. The characteristic duration of the quasi-period for a scale of $\simeq 100$ μm is tens of seconds. Theoretical analysis based, for example, on the nonlinear Landau functional confirms the presence of such dynamics.

Experiments on short-pulsed laser irradiation of a phase separable solution in a cell where convection is suppressed, allow one to determine the position of phase boundaries in the temperature–concentration coordinates. The mechanism of laser-induced quenching of a solution into the metastable region includes light absorption, heating of the solution, its thermal expansion accompanied by a local increase in pressure, and, finally, barodiffusion. The applicability of our optical method for determining the binodal is limited by the efficiency of barodiffusion in the solution. To determine the spinodal position, it is necessary to 'switch on' the mechanism of photo-induced convective mixing caused by optical cavitation.

Barodiffusion in a liquid was observed for the first time. The changes in a liquid caused by barodiffusion are small and difficult to observe. We have managed to observe barodiffu-

sion effects in our experiments owing to the high sensitivity of the solutions near the metastable region to external perturbations.

Acknowledgments
The authors thank F V Bunkin for useful discussions and support and A V Antonov, A V Krasnoslobodtsev, A I Malyarovskiĭ, and Yu P Svirko, in collaboration with whom the main results were obtained.

This work was supported by the Russian Foundation for Basic Research, project No. 96-02-17236.

References

1. Anisimov M A *Kriticheskie Yavleniya v Zhidkostyakh i Zhidkikh Kristallakh* (Critical Phenomena in Liquids and Liquid Crystals) (Moscow: Nauka, 1987) [Translated into English (Philadelphia: GBr Sci. Publ., 1991)]
2. Vedenov A A *Fizika Rastvorov* (Physics of Solutions) (Moscow: Nauka, 1984)
3. Lyakhov G A *Pis'ma Zh. Eksp. Teor. Fiz.* **60** 93 (1994) [*JETP Lett.* **60** 99 (1994)]
4. Bunkin F V et al. *Opt. Acoust. Rev.* **1** 155 (1990)
5. Skripov V P, Skripov A V *Usp. Fiz. Nauk* **128** 193 (1979) [*Sov. Phys. Usp.* **22** 389 (1979)]
6. Cahn J W *J. Chem. Phys.* **42** 93 (1965)
7. Hillert M *Acta Metall.* **9** 525 (1961)
8. Cahn J W *Acta Metall.* **9** 795 (1961)
9. Cahn J W, Hilliard J E *J. Chem. Phys.* **28** 258 (1958)
10. Cahn J W, Hilliard J E *J. Chem. Phys.* **31** 688 (1959)
11. Cahn J W *Trans. Metall. Soc. AIME* **242** 166 (1968)
12. De Gennes P-G *J. Chem. Phys.* **72** 4756 (1980)
13. Pincus P *J. Chem. Phys.* **75** 1996 (1981)
14. Binder K *J. Chem. Phys.* **79** 6387 (1983)
15. Svergun D I, Feĭgin L A *Rentgenovskoe i Neĭtronnoe Malouglovoe Rasseyanie* (X-Ray and Neutron Small-Angle Scattering) (Moscow: Nauka, 1986) [Translated into English (New York: Plenum Press, 1987)]
16. Huang J S, Goldburg W I, Bjerkaas A W *Phys. Rev. Lett.* **32** 921 (1974)
17. Wong N C, Knobler C M *J. Chem. Phys.* **69** 725 (1978); **85** 1972 (1981); *Phys. Rev. A* **24** 3205 (1981)
18. Bates F S, Wiltzius P *J. Chem. Phys.* **91** 3258 (1989)
19. Hashimoto T, Itakura M, Shimidzu N *J. Chem. Phys.* **85** 6773 (1986)
20. Kawasaki K *Progr. Theor. Phys.* **57** 826 (1977)
21. Kawasaki K, Ohta T *Progr. Theor. Phys.* **59** 362 (1978)
22. Furukawa H *Adv. Phys.* **34** 703 (1986); *Phys. Status Solidi A* **123** 497 (1984)
23. Kubota K et al. *J. Chem. Phys.* **97** 9291 (1992)
24. Schwartz A J, Huang J S, Goldburg W I *J. Chem. Phys.* **62** 1847 (1975)
25. Goldburg W I et al. *J. Chem. Phys.* **68** 484 (1978)
26. Schwarts A J, Huang J S, Goldburg W I *J. Chem. Phys.* **63** 599 (1975)
27. Bunkin F V, Podgaetskiĭ V I, Semin V N *Pis'ma Zh. Tekh. Fiz.* **14** 162 (1988) [*Sov. Tech. Phys. Lett.* **14** 72 (1988)]
28. Semin V N *Zh. Fiz. Khim.* **62** 2263 (1988); **63** 1099 (1989)
29. Semin V N, Cand. Dissertation (Moscow: Institute of General Physics, USSR Academy of Sciences, 1990)
30. Atabaev O M et al. *Dokl. Akad. Nauk SSSR* **315** 889 (1990)
31. Van Aarsten J J *Eur. Polymer. J.* **6** 919 (1970)
32. Van Aarsten J J, Smolders C A *Eur. Polymer. J.* **6** 1105 (1970)
33. Van Emmerik P T, Smolders C A, Geymayer W *Eur. Polymer. J.* **9** 309 (1973)
34. Feke G T, Prins W *Macromolecules* **7** 527 (1974)
35. Wiltzius P, Bates F S, Heffner W R *Phys. Rev. Lett.* **60** 1538 (1988)
36. Antonov A V et al. *Zh. Eksp. Teor. Fiz.* **104** 2761 (1993) [*JETP* **77** 266 (1993)]
37. Bunkin N F, Lobeyev A V *J. Chem. Phys.* **104** 6659 (1996)
38. Kafarov V V (Ed.) *Spravochnik po Rastvorimosti* T. 1, kn. 1 (The Handbook of Solubility Data Vol. 1, b. 1) (Leningrad: Nauka, 1976) p. 503
39. Landau L D, Lifshitz E M *Gidrodinamika* (Fluid Mechanics) (Moscow: Nauka, 1986)
40. Bodensohn J, Goldburg W I *Phys. Rev. A* **46** 5084 (1992)
41. Landau L D, Lifshitz E M *Statisticheskaya Fizika* Chast' 1 (Moscow: Nauka, 1976) [Translated into English: *Statistical Physics* Vol. 1 (Oxford: Pergamon Press, 1980)]
42. Gaponov-Grekhov A V, Rabinovich M I *Usp. Fiz. Nauk* **128** 579 (1979) [*Sov. Phys. Usp.* **22** 590 (1979)]
43. Chu B, Schoenes F J, Fisher M E *Phys. Rev.* **185** 219 (1969)
44. Bloembergen N et al. *Phys. Rev. A* **3** 404 (1971)
45. Zel'dovich B Ya, Pilipetskiĭ N F, Shkunov V V *Obrashchenie Volnovogo Fronta* (Optical Phase Conjugation) (Moscow: Nauka, 1985)
46. Lifshitz E M, Pitaevskiĭ L P *Fizicheskaya Kinetika* (Moscow: Nauka, 1979) [Translated into English: *Physical Kinetics* (Oxford, New York: Pergamon Press, 1981)]
47. Gibbs J W *Termodinamicheskie Raboty* (Works on Thermodynamics) (Moscow – Leningrad: Gostekhizdat, 1950)
48. Antonov A V et al. *Zh. Eksp. Teor. Fiz.* **99** 1718 (1991) [*Sov. Phys. JETP* **72** 959 (1991)]
49. Bunkin N F et al. *Kvantovaya Elektron.* (Moscow) **23** 62 (1996) [*Quantum Electron.* **26** 60 (1996)]
50. Bunkin N F, Bunkin F V *Laser Physics* **3** 63 (1993)
51. Bunkin N F et al. *Colloids and Surfaces A* **110** 207 (1996)
52. Vogel A, Lauterborn W, Timm R *J. Fluid Mech.* **206** 299 (1989)